Probing quantum materials with novel scanning tunneling microscopy techniques

Bastiaans, K.M.

2

Amplifier for scanning tunneling microscopy at MHz frequencies

This chapter has been published as *Rev. Sci. Instrum.* **89**, 093709 (2018)

Conventional scanning tunneling microscopy (STM) is limited to a bandwidth of a few kHz around DC. In this chapter, we develop, build and test a novel amplifier circuit capable of measuring the tunneling current in the MHz regime while simultaneously performing conventional STM measurements. This is achieved with an amplifier circuit including a LC tank with a quality factor exceeding 600 and a home-built, low-noise high electron mobility transistor (HEMT). The amplifier circuit functions while simultaneously scanning with atomic resolution in the tunneling regime, i.e. at junction resistances in the range of giga-ohms, and down towards point contact spectroscopy. To enable high signal-to-noise and meet all technical requirements for the inclusion in a commercial low temperature, ultra-high vacuum STM, we use superconducting cross-wound inductors and choose materials and circuit elements with low heat load. We demonstrate the high performance of the amplifier by spatially mapping the Poissonian noise of tunneling electrons on an atomically clean Au(111) surface. We also show differential conductance spectroscopy measurements at 3 MHz, demonstrating superior performance over conventional spectroscopy techniques.

2.1. INTRODUCTION AND MOTIVATION

Possible applications of scanning tunneling microscopy (STM) experiments in the MHz regime include high-frequency differential conductance measurements, scanning spin resonance experiments, and noise spectroscopy on the atomic scale. Conventionally, this is prevented in STM by the combination of a GOhm resistance of the tunnel junction and a capacitor from the cabling which together form a low pass filter in the kHz regime. In this chapter, we build a matching circuit including superconducting inductors and a home-built HEMT that allows us to measure STM currents at MHz frequencies while remaining in tunneling and with atomic resolution. We demonstrate the amplifier's superior performance for both scanning noise spectroscopy and MHz differential conductance measurements.

We start with an introduction to noise spectroscopy. Measurements of electronic noise can yield information in mesoscopic systems that is not present in their time-averaged transport characteristics, including fractional charges in the quantum hall regime [1, 2], the doubling of charge in Andreev processes (see also chapter 4) [3], Coulomb interactions in quantum dots [4–7] and the vanishing of noise in break junctions at the quantum conductance [8]. Generally, the quantity of interest is the deviation of the noise from the Poissonian noise of independent tunneling events of electrons, $S_P = 2e|I|$, with e the electron charge and I the current [9, 10]. Here we define the normalized noise S_n as the ratio between measured (S) and Poissonian (S_P) noise, $S_n = S/S_P$, similar to the Fano factor F. For an uncorrelated electronic liquid, one expects $S_n = 1$; but one can imagine systems where the charge of the carriers is not equal to the electron charge ($q \neq e$) or where the electron flow is strongly correlated. In these cases, the Fano factor will not be equal to unity, i.e. the current noise will be smaller or larger than the Poissonian value even though the time-averaged value of the current will not be influenced. Resolving the noise with atomic precision might provide us with new information in systems with strong electronic correlations or charge aggregations that are not present in the mean current. This is our main motivation to combine noise measurement with scanning probe microscopy.

As for the application of MHz differential conductance measurements, we use a lock-in amplifier as it is done conventionally, but with 3 MHz instead of the more common 400 Hz – 1 kHz. The clear advantage is that in this way, one can perform the spectroscopy measurement in a frequency window where 1/f noise is much lower. In addition to this, we can clearly separate the high and low frequency signal, thus it is, for example, easier to measure in feedback.

Bringing noise measurements to STM in the tunneling regime comes with unique challenges, which prevented any atomic resolution noise measurement in the tunneling regime thus far. The high impedance of the tunnel junction, formed by the few angstroms vacuum gap between the STM tip and sample, is the critical obstacle. To-

gether with the capacitance of the interfacing coax cable, the junction acts as a low pass filter only allowing transmission of signals in the small frequency range [11]. Moreover, conventional amplifiers used in STM also have a limited bandwidth due to a large feedback resistor and unavoidable parasitic capacitances [12]. This conventional STM circuitry limits the bandwidth to detect the tunneling current from DC to a few kHz (Fig. 1a). Possible solutions to this are bootstrapping the amplifier [13–16], or impedance matching [11]. These enabled noise measurements in MOhm tunnel junctions [11, 13, 17, 18], but a GOhm impedance as it is present in many STM experiments still leads to prohibitive losses in the matching circuit.

In this chapter, we report on a new amplifier circuit that allows us to overcome these challenges. The requirements for our amplifier were: (i) the amplifier should not interfere with traditional STM measurements, (ii) it should work in the GOhm regime, (iii), it has to be possible to easily implement the amplifier in a commercial STM, (iv) it has to be compatible with UHV, implying low outgassing so that the system can be baked and ultra-high- (cryogenic) vacuum can be achieved.

Our key figures of merit are: (i) the low noise of the circuit, (ii) the most efficient separation of high and low frequency signals, and (iii) the highest possible Q factor of the resonator for highest amplification at 3 MHz.

This chapter is structured as follows. Noise in a STM junction is discussed in section 2.2. A block diagram of the newly developed system for noise-spectroscopy measurements in STM is presented in section 2.3.a, followed by a discussion on the requirements for implementing such techniques in STM. Section 2.3.b describes the realization of this new amplifier. A demonstration measurement on an Au(111) surface is presented in section 2.4. Differential conductance measurements with MHz voltage modulation are discussed in section 2.5.

2.2. NOISE SOURCES IN STM

We start by considering the types of unwanted noise present in a STM setup: mechanical noise, thermal (Johnson) noise, amplifier noise, and flicker (1/f) noise.

They have distinguishable frequency dependences, as shown in Fig. 2.1.a. First, flicker noise or 1/f noise, which is present in almost all electronic devices. The power spectral density of this low-frequency phenomenon is inversely proportional to the frequency and is related to slow resistance fluctuations modulated by temperature variations. Second, noise induced by mechanical vibrations transferred to the junction, where this mechanical noise is converted to current noise. Both noise sources are usually present in the range from DC to a few kHz, indicated by the blue shaded area in Fig. 2.1.a. This emphasizes that the low frequency regime should be avoided

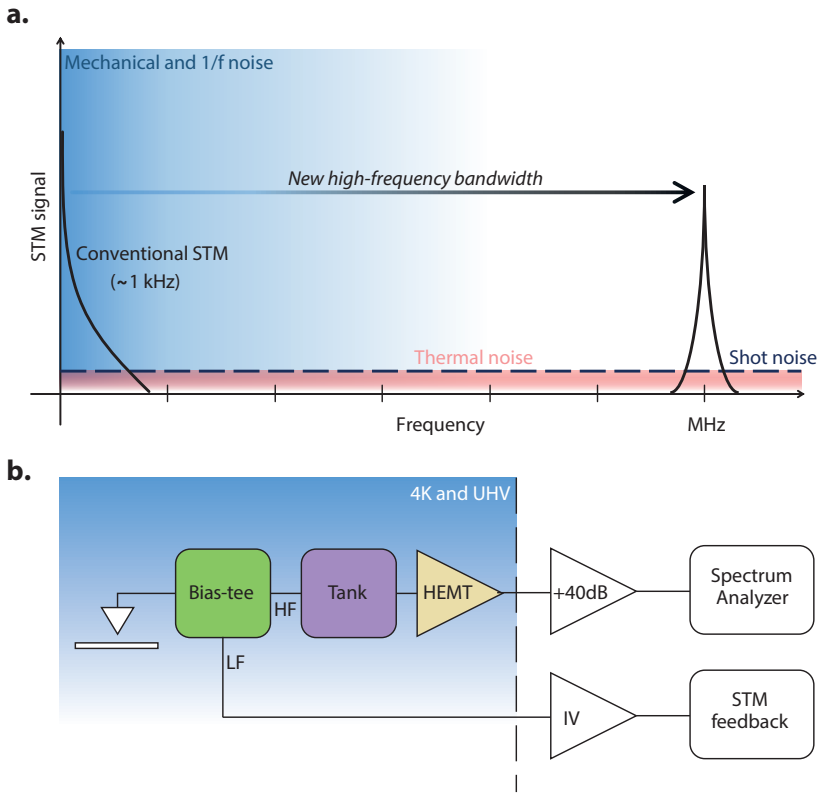

Figure 2.1: **Noise in scanning tunneling microscopy (STM). a.** The different noise sources in STM and their frequency dependence are depicted in this schematic plot. At low frequencies mechanical and $1/f$ noise dominate (indicated by blue region), in this region conventional STM is sensitive. To measure shot noise in the tunnel junction we need to create a new bandwidth at high-frequency. Here thermal noise and shot noise are the most dominant noise sources, since they are independent of frequency. **b.** Requirements for the newly built amplifier for combining STM and noise-spectroscopy. Crucial components are highlighted: i) the bias-tee (green) that separates the low and high frequency signals. ii) tank circuit (purple). iii) High electron mobility transistor (HEMT, indicated in yellow) to amplify the high-frequency signal. Both the low and high frequency signals have additional room temperature amplification and detection (white).

and illustrates the disadvantages of the conventional STM bandwidth.

At higher frequencies, the current fluctuations are dominated by thermal noise and shot noise, both of which are informative about the sample. In principle, both phenomena are frequency independent (white noise), and thus are also present at lower frequencies, where the total noise power is dominated by the other contributions. Thermal (also called Johnson-Nyquist) noise is the thermodynamic electronic noise in any conductor with a finite resistance R; its power spectral density is constant throughout the frequency spectrum, $S = 4k_B T$, where k_B is Boltzmann's constant and T is the temperature. Since thermal noise in a conductor is proportional to the temperature, it can be lowered by reducing the temperature. It can be distinguished from shot noise at zero current, where the latter vanishes.

Our goal is thus to increase the bandwidth and move it to higher frequencies, all whilst retaining the conventional capabilities and staying in the tunneling regime.

2.3. AMPLIFIER AND CIRCUIT

2.3.1. GENERAL IDEA

To achieve the requirements and goals of section 2.1 while avoiding the unwanted noise sources described in section 2.2, we develop a resonance circuit based amplifier including a resonator-based bias-tee.

We follow the principle of amplifier circuits built for noise spectroscopy measurements in mesoscopic systems [19–22] but we modify it to work for high junction resistances in the GOhm regime and to be compatible with STM. Figure 2.1.b shows a block diagram of the amplifier circuit combined with STM. First, a bias-tee (green) separates the low- and high-frequency signals coming from the STM junction. The low-frequency part is needed for the STM feedback loop, where the current is converted to a voltage by a transimpedance amplifier at room temperature. To separate the high frequency, one could use a bias-tee consisting of an inductor in one arm and a capacitor in the other one. However, as we still need a kHz bandwidth in the low frequency branch and as we want to minimize losses of the high frequency signal, we use a resonator based bias-tee.

The high-frequency part of the signal is then passed through the parallel RLC circuit (tank, indicated in purple Fig. 2.1.b), which converts current to voltage at the resonance frequency of the tank circuit $f_0 = (2\pi\sqrt{LC})^{-1}$. The voltage over the tank circuit is detected by the gate of a high electron mobility transistor (HEMT, indicated in yellow Fig. 2.1.b) with very low input referred voltage [23, 24] and current noise, operating at the base temperature ($T \sim 3.3$ K in this chapter) of the STM. Through

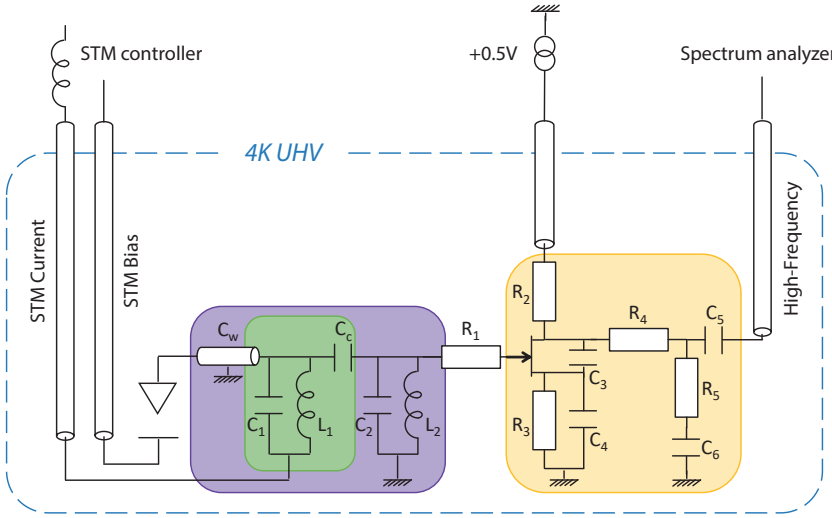

Figure 2.2: **Circuit diagram of the newly developed amplifier for scanning noise spectroscopy.** The colored boxes (green, purple and yellow) highlight specific parts of the amplifier corresponding to Fig. 2.1.b.

the transimpedance of the HEMT, the voltage fluctuations at its gate are converted into current fluctuations. These are measured over a 50 Ω resistor to finalize the impedance transformation. Note that while the voltage/current gain of the amplifier is of order unity, the gain of power is considerable. A 50 Ω coaxial line connects the amplifier circuit to a commercial 40 dB current amplifier at room temperature. Finally, the signal line is terminated by the 50 Ω input impedance of the spectrum analyzer.

2.3.2. CIRCUIT ELEMENTS AND PRINTED CIRCUIT BOARD DESIGN

The heart of the circuit is built on a ceramic printed circuit board (Rogers Corp TMM10i, selected for the very low outgassing properties) as depicted in Fig. 2.2 and described below. Figure 2.2 shows the circuit schematics of the amplifier. The board is located close to the STM head, at the base temperature of the liquid He 4 cryostat (Unisoku USM1500).

The input of the amplifier is connected to the STM tip via a coaxial cable (silver plated Cu mini-coax CW2040-3650F) with a total capacitance between inner and outer conductor of C_w = 30 pF. The bias-tee (indicated by green shading) and tank (purple shading) combination is formed by two home-built superconducting Niobium inductors $L_1 = L_2 = 66\,\mu H$ coupled by capacitors C_c = 100 pF (Murata GRM 0805-size surface mount). The low-frequency transmission of the bias-tee is shown in Fig.

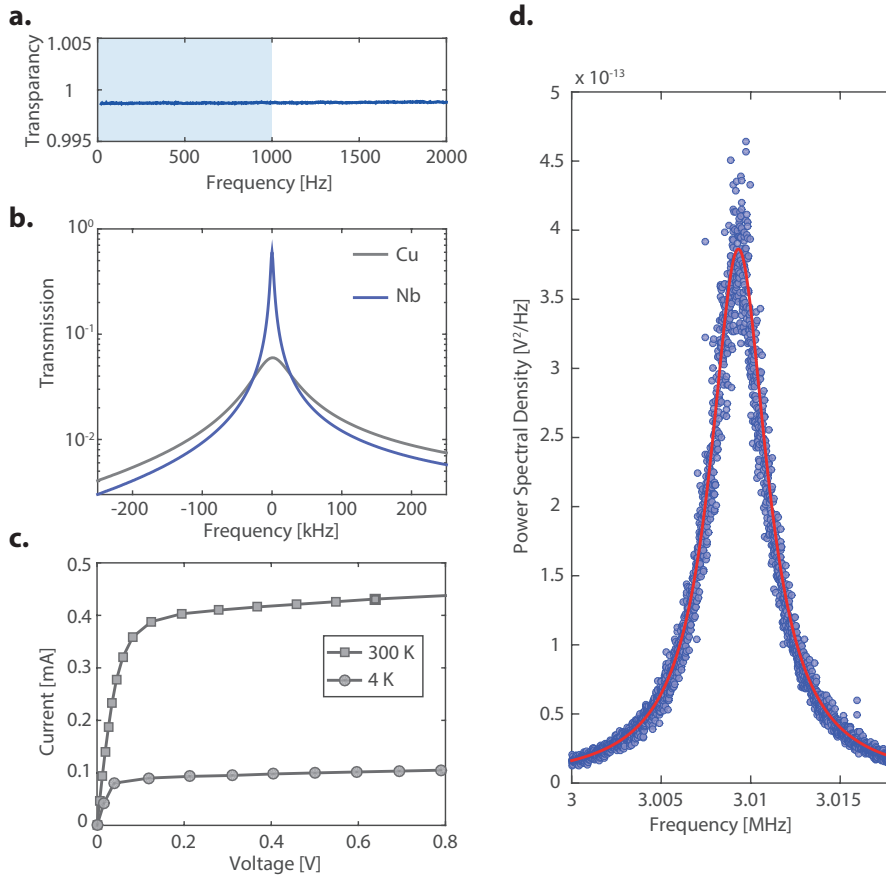

Figure 2.3: **a.** Low-frequency signal used for the STM feedback system. The transparency is close to 1 and flat from DC up to 2 kHz. Bandwidth of the FEMTO transimpedance amplifier (1kHz) is indicated by the shaded blue area. **b.** Transmission of a home-built copper (grey) and superconducting niobium (blue) inductor resonator circuit. The latter showing a much higher quality factor. **c.** Current-voltage characteristics of the high electron mobility transistor (HEMT) at 300 K and LHe temperatures. **d.** Power spectral density measured in a small bandwidth around the resonance frequency of the tank circuit (3.009 MHz). Blue dots are measured data points, red curve corresponds to a circuit diagram fit.

2.3.a, measured at low temperature. The flat transfer function in the frequency range of the Femto IV amplifier (1 kHz, blue shaded are in Fig. 2.3.a) ensures that this amplification scheme can be used for the STM feedback system.

The resonance circuit is formed by the self-resonance of the superconducting Nb inductors in combination with the coaxial cable C_w, providing a resonance frequency of 3.009 MHz. Parallel self-capacitances of the Nb inductors are also shown in Fig. 2.2.a, C_1 = 15 pF and C_2 = 15 pF. The Niobium inductors are made by cross-winding annealed Nb wire of 100 μm in diameter around a customized ceramic (macor) core. We choose superconducting Nb inductors to enhance the quality factor of the resonator, increasing current-to-voltage amplification at resonance. At 4 K, the Nb inductors show a high quality factor of Q = 600, 50 times larger than similarly made Cu inductors (Q = 12), see Fig. 2.3.b. The Nb inductors are covered by a Nb shield to minimize Eddy current damping, ensuring the highest possible quality factor Q.

The high-impedance part of the amplification scheme (tank circuit coupled to STM junction) is matched to the 50 Ω impedance of the spectrum analyzer by a home-built low-noise high electron mobility transistor (HEMT) made using molecular beam epitaxy. These specially designed HEMT's have a carrier mobility of $48 m^2/Vs$ and can reach unprecedented low noise levels at 1 MHz with a noise voltage of $0.25\, nV/\sqrt{Hz}$ and a noise current of $2.2\, fA/\sqrt{Hz}$, under deep cryogenic conditions (≤ 4.2 K), and with an input capacitance of about 5 pF [23, 24]. In addition, components C_3 = 10 pF, R_1 = 10 Ω and R_4 = 10 Ω are placed close to the HEMT case to improve its stability.

The operation point of the HEMT is determined by R_2 and R_3 and the supply voltage. Since we aim to have a very low power dissipation we choose R_2 = 1 kΩ to give a saturation current of the HEMT of a few tenths of mA. To ensure linear gate voltage to current conversion we operate the HEMT is in saturation. We measured the drain current as function of drain-source voltage at room temperature and 4 K by varying the supply voltage, as depicted in Fig. 2.3.c. In the following demonstration the HEMT is biased in saturation at V = 0.5 V.

The voltage fluctuations in the 50 Ω line are amplified at room temperature by a +40 dB current amplifier with an input voltage noise of $310\, pV/\sqrt{Hz}$ (Femto HSA-X-1-40) and is finally terminated by the 50 Ω input impedance of a Zurich Instruments MFLI digital spectrum analyzer. The power spectral density measured at the input of the spectrum analyzer is plotted in Fig. 2.3.d where the blue dots are the measured data points and the red curve represents a circuit diagram fit.

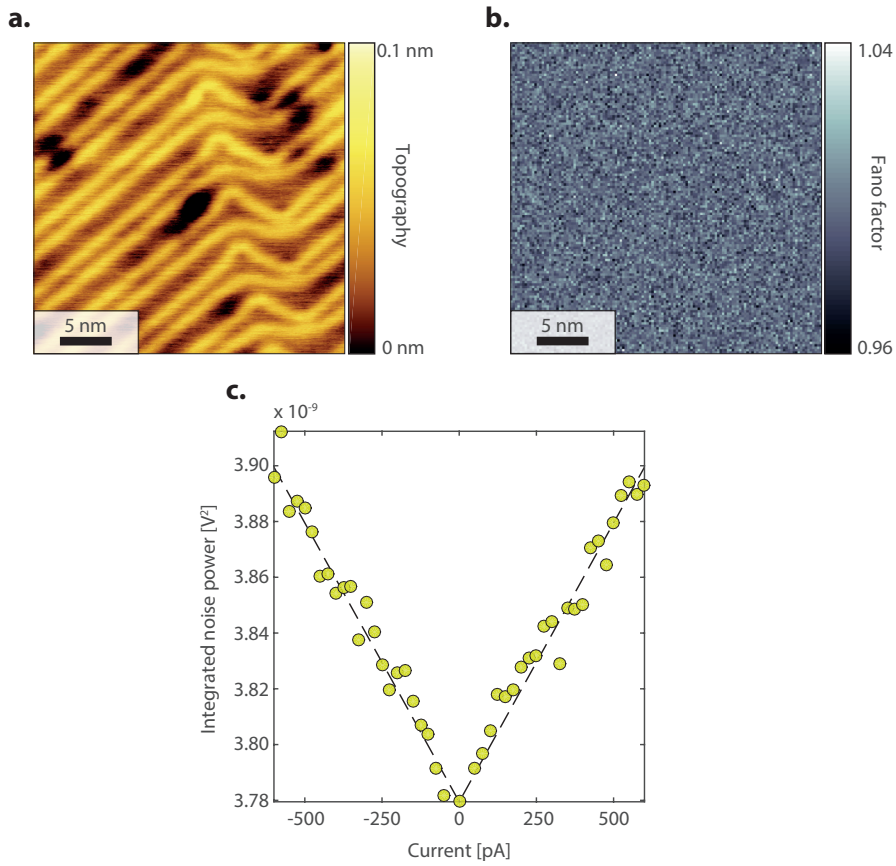

Figure 2.4: **Benchmark of noise-sensitive measurements on a gold on mica sample. a.** An atomically resolved STM topographic image of the Au(111) surface on a 30 nm field of view, the 'herringbone' reconstruction is clearly visible. (Setup conditions bias: 100 mV, current set point: 100 pA). **b.** Spatially resolved noise map at 500 mV, 500 pA in the same field of view as Fig 2.4.a, acquired in 48 hours. It shows homogenous Poissonian (Fano = 1) noise at all locations. Here the Fano factor is extracted as $F_{measured} = (S(500pA) - S(0pA))/(2e500pA)$. **c.** Single point noise spectrum acquired at a random location in Fig. 2.4.b. The tunnel junction resistance is kept fixed to 1 GOhm. The dashed line indicates Poissonian shot noise $F = 1$.

2.4. NOISE SPECTROSCOPY PERFORMANCE ON ATOMICALLY AU(111)

To demonstrate the simultaneous use of the STM feedback system and noise sensitive measurements in the tunneling regime, we performed noise spectroscopy measurements on a gold on mica sample. We believe that the Au(111) surface is most ideal for characterizing our noise-sensitive measurement since the sample is metallic thus any electron correlations are negligible. Figure 2.4.a depicts an atomic-resolution image of the Au(111) terminated surface on a 30 nm field of view, the characteristic 'herringbone' reconstruction is clearly visible.

In the same field of view we performed noise-spectroscopy measurements to resolve the current noise with atomic-scale resolution. Even though several topographic features can be observed, the spatially resolved noise map (Fig. 2.4.b) exhibits homogeneous contrast, as is expected for a classical uncorrelated flow of electrons between sample and tip. The 128 × 128 pixel noise map was acquired in circa 48 hours.

The single point noise spectra (Fig. 2.4.c) acquired at randomly chosen sites always show a linear increase of the noise with increasing current for a typical tunneling junction resistance (1GOhm). The linear increase of the noise is a unique characteristic of shot noise in the junction.

2.5. MHZ DIFFERENTIAL CONDUCTANCE MEASUREMENTS

A second application for our amplifier circuit is to measure differential conductance (dI/dV) which is proportional to the local density of states in a frequency range where 1/f noise is suppressed. In conventional STM differential conductance measurements, a voltage modulation has to be applied in the DC - 1 kHz range, now we can also perform dI/dV measurements at 3 MHz. At this frequency, 1/f (and other) noise should be considerably lower, as we discussed in section 2.2, Fig. 2.1.a. Therefore, we expect that differential conductance measurements performed at 3 MHz will show superior performance over conventional spectroscopic-imaging STM measurements.

Figure 2.5.a shows that we can resolve the 3 MHz voltage modulation, applied to the sample, within the tank bandwidth; the sharp peak in Fig. 2.5.a (0.5 mV modulation amplitude at 3.009 MHz) is 6 orders of magnitude higher than the background. To verify that the signal to noise ratio of MHz differential conductance measurements is higher than state-of-the-art STM techniques, we will compare the two by the means of a demonstration measurement on a Pb(111) sample using a Pb-coated PtIr tip at 3.3 K.

First, we compare the differential conductance measured over a period of 10 s in tunneling (6 mV, 200 pA) with the feedback disabled. In this way we can check the influence of slow (1/f) fluctuations on the differential conductance signal. Comparing the conventional dI/dV measurement (Fig. 2.5.b, measured using the RHK R9 STM controller) with the MHz measurement (Fig. 2.5.c, measured using the Zurich Instruments MFLI) reveals that the former is subject to much severe low-frequency fluctuations than the latter. This directly translates into a higher quality dI/dV spectrum, as can be seen by comparing the 3.009 MHz dI/dV spectrum (Fig. 2.5.e) to the one measured at 887 Hz (Fig. 2.5.d).

2.6. CONCLUSIONS AND OUTLOOK

In this chapter we have shown how we have built a low temperature, low noise amplifier to measure the current (fluctuations) in a STM setup at a MHz frequency. We used two superconducting Nb inductors to form a bias-tee and tank resonator coupled to a home-built, low-noise HEMT which is essential for the impedance matching to 50 Ω coax cable. We demonstrated the performance of this amplifier by performing noise spectroscopy measurements on an Au(111) surface, showcasing simultaneous visualization of the surface topology and atomically resolved noise maps. We further demonstrated that the amplifier allows to measure differential conductance spectra at 3 MHz where $1/f$ noise is strongly suppressed.

The development of this MHz amplifier, along with recent developments from other research groups [25], directly opens new paths to explore many-body correlation effects in quantum materials. As we will discuss in the next chapter, we use MHz noise-spectroscopy in a STM setup to discover slow MHz timescale charge trapping behavior in a cuprate high-temperature superconducting, providing unique insights in the so-called 'c-axis mystery' in these materials. In chapter 4 we will use the same noise-spectroscopy technique to demonstrate the doubling of the noise due to Andreev reflections in a Josephson STM, and elucidate its future potential. Further, the developments presented in this chapter also open additional possibilities to probe electron spin resonances (ESR) in STM. ESR often leads to periodic processes and equilibration times in the MHz to GHz regime [26, 27]. These can be measured impedance matched with the presented amplifier instead of measuring indirect effects on the DC current. This could be further improved by guiding the microwave signal directly on the tip with coplanar waveguides, as suggested recently [28]. Finally, one could imagine that the thermal noise, introduced here as an unwanted noise source, could yield information about the sample via cross-correlation noise [29].

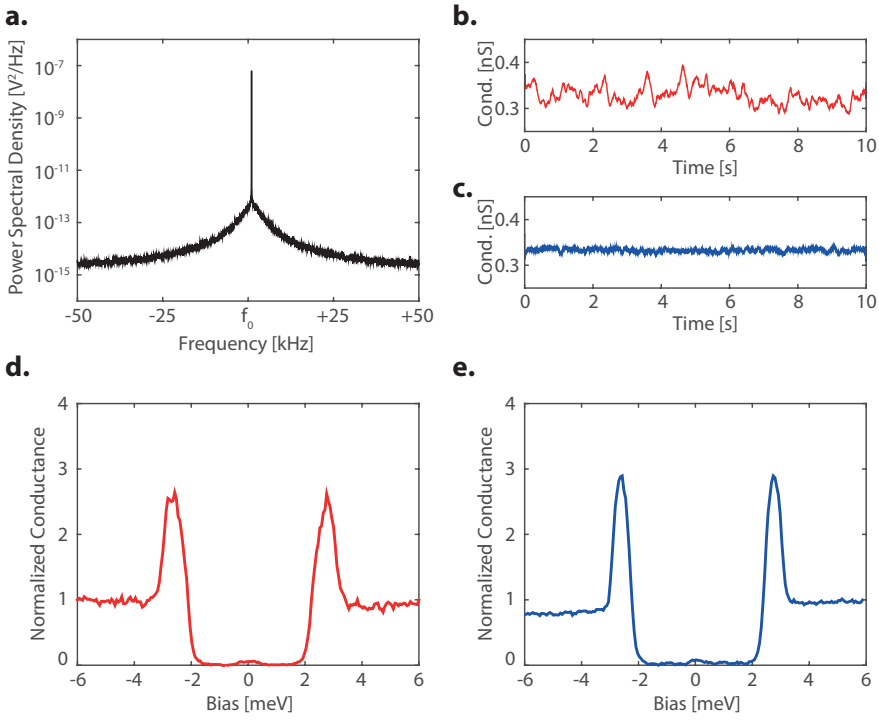

Figure 2.5: **MHz differential conductance. a.** Power spectrum obtained around the resonance peak. The modulation signal for the lock-in measurement is applied at the resonance frequency (3.009 MHz). **b.** Differential conductance measured over time at 887 Hz. A voltage modulation of 0.5 mV is used and feedback is disabled. **c.** Differential conductance measured over time at the resonance frequency (3.009 MHz) under similar conditions as figure 2.5.b. **d.** Differential conductance spectrum obtained with a 0.5 mV voltage modulation at 887 Hz (time constant 2 ms) on a Pb(111) surface at a base temperature of 3.3 K. **e.** Differential conductance spectrum obtained at the resonance frequency (3.009 MHz, time constant 3.5 μs) obtained under the same conditions as figure 2.5.d.

BIBLIOGRAPHY

[1] R. De-Picciotto, M. Reznikov, M. Heiblum, V. Umansky, G. Bunin, and D. Mahalu, *Direct observation of a fractional charge,* Nature **389**, 162 (1997).

[2] L. Saminadayar, D. C. Glattli, Y. Jin, and B. Etienne, *Observation of the e/3 fractionally charged laughlin quasiparticle,* Phys. Rev. Lett. **79**, 2526 (1997).

[3] Y. Ronen, Y. Cohen, J.-H. Kang, A. Haim, M.-T. Rieder, M. Heiblum, D. Mahalu, and H. Shtrikman, *Charge of a quasiparticle in a superconductor,* PNAS **113**, 1743 (2016).

[4] A. Thielmann, M. H. Hettler, J. König, and G. Schön, *Cotunneling current and shot noise in quantum dots,* Phys. Rev. Lett. **95**, 146806 (2005).

[5] E. Onac, F. Balestro, B. Trauzettel, C. F. J. Lodewijk, and L. P. Kouwenhoven, *Shot-noise detection in a carbon nanotube quantum dot,* Phys. Rev. Lett. **96**, 026803 (2006).

[6] G. Iannaccone, G. Lombardi, M. Macucci, and B. Pellegrini, *Enhanced shot noise in resonant tunneling: Theory and experiment,* Phys. Rev. Lett. **80**, 1054 (1998).

[7] S. Oberholzer, E. V. Sukhorukov, C. Strunk, C. Schönenberger, T. Heinzel, and M. Holland, *Shot noise by quantum scattering in chaotic cavities,* Phys. Rev. Lett. **86**, 2114 (2001).

[8] H. E. Van den Brom and J. M. Van Ruitenbeek, *Quantum suppression of shot noise in atom-size metallic contacts,* Phys. Rev. Lett. **82**, 1526 (1999).

[9] Y. M. Blanter and M. Büttiker, *Shot noise in mesoscopic conductors,* Physics Reports **336**, 1 (2000).

[10] Y. M. Blanter and M. Büttiker, *Transition from sub-poissonian to super-poissonian shot noise in resonant quantum wells,* Physical Rev. B **59**, 10217 (1999).

[11] U. Kemiktarak, T. Ndukum, K. C. Schwab, and K. L. Ekinci, *Radio-frequency scanning tunnelling microscopy,* Nature **450**, 85 (2007).

[12] C. J. Chen, *Introduction to scanning tunneling microscopy*, Vol. 4 (Oxford University Press on Demand, 1993).

[13] H. Birk, M. J. M. De Jong, and C. Schönenberger, *Shot-noise suppression in the single-electron tunneling regime,* Phys. Rev. Lett. **75**, 1610 (1995).

[14] H. Birk, K. Oostveen, and C. Schönenberger, *Preamplifier for electric-current noise measurements at low temperatures,* Rev. Sci. Instrum. **67**, 2977 (1996).

[15] M. J. Rost, L. Crama, P. Schakel, E. van Tol, G. B. E. M. van Velzen-Williams, C. F. Overgauw, H. ter Horst, H. Dekker, B. Okhuijsen, M. Seynen, A. Vijftigschild, P. Han, A. J. Katan, K. Schoots, R. Schumm, W. van Loo, T. H. Oosterkamp, and J. W. M. Frenken, *Scanning probe microscopes go video rate and beyond,* Rev. Sci. Instrum. **76**, 053710 (2005).

[16] H. Mamin, H. Birk, P. Wimmer, and D. Rugar, *High-speed scanning tunneling microscopy: Principles and applications,* Journal of applied physics **75**, 161 (1994).

[17] A. Burtzlaff, A. Weismann, M. Brandbyge, and R. Berndt, *Shot noise as a probe of spin-polarized transport through single atoms,* Phys. Rev. Lett. **114**, 016602 (2015).

[18] A. Burtzlaff, N. L. Schneider, A. Weismann, and R. Berndt, *Shot noise from single atom contacts in a scanning tunneling microscope,* Surface Science **643**, 10 (2016).

[19] L. DiCarlo, Y. Zhang, D. T. McClure, C. M. Marcus, L. N. Pfeiffer, and K. W. West, *System for measuring auto-and cross correlation of current noise at low temperatures,* Rev. Sci. Instrum. **77**, 073906 (2006).

[20] T. Arakawa, Y. Nishihara, M. Maeda, S. Norimoto, and K. Kobayashi, *Cryogenic amplifier for shot noise measurement at 20 mk,* Applied Physics Letters **103**, 172104 (2013).

[21] M. Hashisaka, Y. Yamauchi, S. Nakamura, S. Kasai, K. Kobayashi, and T. Ono, *Measurement for quantum shot noise in a quantum point contact at low temperatures,* in *Journal of Physics: Conference Series*, Vol. 109 (IOP Publishing, 2008) p. 012013.

[22] A. M. Robinson and V. I. Talyanskii, *Cryogenic amplifier for 1 mhz with a high input impedance using a commercial pseudomorphic high electron mobility transistor,* Rev. Sci. Instrum. **75**, 3169 (2004).

[23] Q. Dong, Y. X. Liang, D. Ferry, A. Cavanna, U. Gennser, L. Couraud, and Y. Jin, *Ultra-low noise high electron mobility transistors for high-impedance and low-frequency deep cryogenic readout electronics,* Applied Physics Letters **105**, 013504 (2014).

[24] Y. Jin, Q. Dong, U. Gennser, L. Couraud, A. Cavanna, and C. Ulysse, *Ultra-low noise cryohemts for cryogenic high-impedance readout electronics: Results and applications,* in *2016 13th IEEE International Conference on Solid-State and Integrated Circuit Technology (ICSICT)* (IEEE, 2016) pp. 342–345.

[25] F. Massee, Q. Dong, A. Cavanna, Y. Jin, and M. Aprili, *Atomic scale shot-noise using cryogenic mhz circuitry,* Rev. Sci. Instrum. **89**, 093708 (2018).

[26] S. Loth, M. Etzkorn, C. P. Lutz, D. M. Eigler, and A. J. Heinrich, *Measurement of fast electron spin relaxation times with atomic resolution,* Science **329**, 1628 (2010).

[27] S. Baumann, W. Paul, T. Choi, C. P. Lutz, A. Ardavan, and A. J. Heinrich, *Electron paramagnetic resonance of individual atoms on a surface,* Science **350**, 417 (2015).

[28] M. Leeuwenhoek, R. A. Norte, K. M. Bastiaans, D. Cho, I. Battisti, Y. M. Blanter, S. Gröblacher, and M. P. Allan, *Nanofabricated tips as a platform for double-tip and device based scanning tunneling microscopy,* Nanotechnology,*in press* (2019).

[29] H. Grabert, *Dynamical coulomb blockade of tunnel junctions driven by alternating voltages,* Phys. Rev. B **92**, 245433 (2015).